ELSEVIER

Carbohydrate Research 273 (1995) 11–26

CARBOHYDRATE RESEARCH

A reinvestigation towards the conformation of methyl α-D-mannopyranosyl-(1 → 6)-α-D-mannopyranoside by a combined ROE and molecular dynamics analysis

Bertina A. Spronk, Alfonso Rivera-Sagredo [1], Johannis P. Kamerling, Johannes F.G. Vliegenthart *

Bijvoet Center, Department of Bio-Organic Chemistry, Utrecht University, P.O. Box 80.075, NL-3508 TB Utrecht, The Netherlands

Received 7 November 1994; accepted 19 January 1995

Abstract

Conformational analysis of α-D-Man*p*-(1 → 6)-α-D-Man*p*1-OMe, by a combination of extensive molecular dynamics calculations in water and ROE buildup series, afforded two main minima, namely, $\phi/\psi = 95/-178$ and $\phi/\psi = 140/-185$. Transitions between these minima are observed, which have not previously been demonstrated using other approaches. In contrast to literature data for the glycosidic linkage, describing equal populations of both the *gg* and the *gt* rotamers, it was found that the *gg* conformer is present to ca. 96%. The non-reducing mannosyl unit showed approximately a 1:1 ratio for the *gg*:*gt* equilibrium, in accordance with earlier reports.

Keywords: Conformation; Molecular dynamics; NMR spectroscopy; Mannose; α-(1 → 6) Glycosidic linkage

1. Introduction

In the framework of our studies focused on the determination of the overall structure of the oligomannose and hybrid type glycans, it appeared necessary to evaluate literature data concerning the conformation of methyl α-D-mannopyranosyl-(1 → 6)-α-D-

[1] Present address: SmithKline Beecham, Centro de Investigacíon Básica, TRES CANTOS-Madrid, Spain.

* Corresponding author.

SSDI 0008-6215(95)00061-5

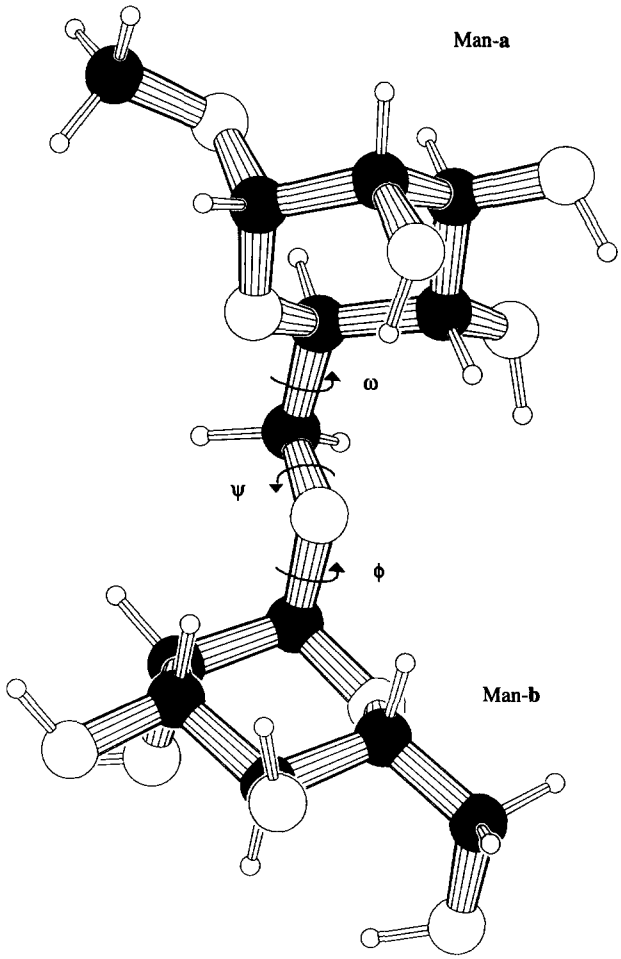

Fig. 1. α-D-Man*p*-(1 → 6)-α-D-Man*p*1-OMe (**1**) showing ω, ϕ, and ψ. The 6-linked mannose residue is denoted Man-**a**, and the terminal mannosyl group Man-**b**.

mannopyranoside. The (1 → 6) linkage is crucial for the conformational analysis of larger glycans, mainly because of the additional torsional angle ω (Fig. 1).

Several studies have been performed to establish the conformation of the α-D-Man-(1 → 6)-α-D-Man moiety, investigating the disaccharide itself [1–3] or as part of a larger oligomannose or hybrid type of structure [4,5]. To this end commonly used techniques such as molecular mechanics calculations (MM) [3] and ^{1}H NMR NOE measurements [1] or a combination of these two [2,4,5] have been applied. With respect to α-D-Man*p*-(1 → 6)-α-D-Man*p*1-OMe (**1**) an equal probability for the *gg* and the *gt* rotamer, and a ϕ/ψ minimum of 60/150 have been found [1,4]. The values of the coupling constants $J_{5,6b}$ (4.5 Hz) and $J_{5,6a}$ (1.8 Hz) were determined by comparing the ^{1}H NMR data of **1** with those of α-D-Man*p*-(1 → 6)[α-D-Man*p*-(1 → 3)]-α-D-Man*p*1-OMe. On the basis

of a molecular dynamics (MD) simulation of α-D-Man*p*-(1 → 6)-α-D-Man (**2**) in vacuum for 10 ps, together with ^{1}H NMR NOE experiments and potential energy calculations, an averaged ϕ/ψ combination of 95/166 was observed for the MD trajectory [2]. Since these studies, greater computational power has become available, and the resolution and possibilities of NMR have increased rapidly.

To gain insight into the flexibility across the interglycosidic linkages ([6], and references cited therein), MD simulations in the present study were performed in water during 500 ps. The rotamer populations for the exocyclic (hydr)oxymethyl groups were obtained from the relevant coupling constants via an undecoupled heteronuclear multiple-quantum correlation (HMQC) experiment, and the preferred ϕ/ψ minima were determined using a combination of NMR ROE buildup series and MD.

2. Experimental

NMR spectroscopy.—α-D-Man*p*-(1 → 6)-α-D-Man*p*1-OMe was exchanged twice in 99.9% D_2O (Isotec Inc., Miamisburg, USA) with intermediate lyophilization, and finally dissolved in 99.96% D_2O. All spectra were recorded on a Bruker AMX-500 spectrometer equipped with an X32 console (Bijvoet Center, Department of NMR Spectroscopy, Utrecht University). Chemical shifts are expressed in ppm by reference to internal acetone in D_2O (δ 2.225). The HOD signal was suppressed by presaturation during 1.0 s.

2D ROE measurements were carried out at 285 K using the Time Proportional Phase Increment (TPPI) method [7] to acquire phase-sensitive spectra [8,9]. The carrier frequency was placed at the left-hand side of the spectrum at δ 5.570, and the power of the spin-lock pulse corresponded to a 90° degree pulse of 100 μs. Mixing times used were 50, 100, 150, 200, 300, or 400 ms. The spectral width was 3000 Hz in each dimension, and 4K data points were recorded in 512 increments.

The natural-abundance proton-detected $^1H - ^{13}C$ HMQC spectrum was recorded at 285 K without decoupling during acquisition [10,11]. The spectral width was 2717 Hz in the ^{1}H domain and 7350 Hz in the ^{13}C domain, whereas 4K datapoints and 650 experiments were zero-filled to a 4K × 1K data matrix.

The spectra were processed on a 4D/35 Silicon Graphics station with the TRITON NMR software package (R. Boelens and R. Kaptein, Bijvoet Center, Department of NMR Spectroscopy). The data were multiplied with a $\pi/2.2$-shifted square sine bell in the ω_2 time domain, and in the ω_1 time domain with a $\pi/2.5$-shifted square sine bell. A third-order polynomal baseline correction was applied after the first Fourier transformation, and a fourth-order polynomal baseline correction after the second Fourier transformation. The ROE cross-peaks were integrated by summation of the intensities within a defined rectangle, with a baseplane through this rectangle. Overlapping ROE peaks were integrated to obtain one overall value.

Nomenclature.—The torsional angles ϕ, ψ, and ω are defined according to IUPAC conventions [12]: ϕ as (O-5$_b$, C-1$_b$, O-6$_a$, C-6$_a$), ψ as (C-1$_b$, O-6$_a$, C-6$_a$, C-5$_a$), and ω (determining the rotamer population) as (O-6, C-6, C-5, C-4).

MD simulation.—The MD simulation was performed using the GROMOS program [13] and its standard force field for carbohydrates [14]. The united atom approach was used for aliphatic carbon atoms. Positions of the corresponding hydrogen atoms were calculated after simulation, for each timestep, by using tetrahedral geometry and a C–H bond length of 1.1 Å. For the simulation α-D-Man*p*-(1 → 6)-α-D-Man*p*1-OMe was placed in a computational octahedral periodic box containing ca. 310 water molecules, and the calculations were carried out at constant temperature (300 K) with a time step of 2 fs, using a 4D/35 Silicon Graphics workstation. All bond lengths were constrained using the SHAKE method [15]. Temperature and pressure in the system were kept constant with relaxation times of 0.1 and 0.5 ps, respectively. Nine runs of 500 ps were performed, each with one of the nine different $\phi/\psi/\omega$ minima encountered in the database [3] as starting structures, namely, Egg1 (70/−170/60), Egg2 (75/100/60), Egg3 (150/−115/60), Egg4 (160/120/60), Egt1 (70/−170/180), Egt2 (75/90/180), Egt3 (150/−100/180), Egt4 (165/115/180), and Egt5 (105/−80/180). The numbering of the minima reflects the order of increasing potential energy.

Rotamer populations.—The rotamer populations were calculated using a Karplus equation as described in [16], with a modified torsional angle set for ω 53° (*gg*), ω −175° (*gt*), and for ω −65° (*tg*) [17].

CROSREL program.—CROSREL [18,19] provides a full relaxation rate matrix approach for the analysis of ROE spectra. This program can calculate theoretical intensities using models derived from MD simulations, and these intensities can be compared with observed ROE intensities. The quality of the structure is judged based on a weighted *R*-factor [19,20]

$$R_w = \left\{ \frac{\sum_{i=1}^{n}\sum_{j=1}^{n}\sum_{\tau_m}^{m} w_{ij}(\tau_m)\left[A_{ij}^{\mathrm{calc}}(\tau_m) - A_{ij}^{\mathrm{obs}}(\tau_m)\right]^2}{\sum_{i=1}^{n}\sum_{j=1}^{n}\sum_{\tau_m}^{m} w_{ij}(\tau_m)\left[A_{ij}^{\mathrm{obs}}(\tau_m)\right]^2} \right\}^{1/2} \quad (1)$$

comparing the calculated intensities from the model structure $A^{\mathrm{calc}}(\tau_m)$, to the observed cross-peak intensities, $A^{\mathrm{obs}}(\tau_m)$. The weights $w_{ij}(\tau_m)$ are defined as

$$w_{ij}(\tau_m) = \frac{1}{A_{\mathrm{noise}} + |A_{ij}^{\mathrm{obs}}(\tau_m)|} \quad (2)$$

wherein A_{noise} is the estimated background error of peak integration. This weighting function gives appropriate weight to the smaller ROE intensities, which are usually the most conformationally sensitive. The various trajectories are analysed using $< r^{-3} >$ or $< r^{-6} >$ distance averaging. The general spectral density function used is

$$J_n(\omega) = < r^{-6} > \frac{\tau_c}{1 + n^2\omega^2\tau_c^2} \quad (3)$$

In Eq. 3 $< r^{-3} >^2$ can also be substituted for $< r^{-6} >$. Information about the overall motion (τ_c) is obtained using intraresidue cross-peaks. Furthermore, CROSREL has been used to combine several sets of averaged trajectories with different ratios to

calculate *R*-values. The program corrects for the offset dependence of the ROE experiment, and for HOHAHA magnetisation transfer during the spin-lock period.

Summation of overlapping peaks is implemented; this feature is especially important for carbohydrates, since overlap is frequently observed. In order to compare the calculated and the observed data, scaling is necessary. By integration of all peaks, including the diagonal peaks, extrapolation to the equilibrium magnetisation (which is the diagonal intensity at $\tau_m = 0$) is possible. The equilibrium magnetisation is calculated from the columns of the 2D spectrum because of the offset dependence in the rows.

3. Results

The ^{1}H and ^{13}C NMR chemical shifts of α-D-Man*p*-(1 → 6)-α-D-Man*p*1-OMe (**1**), abbreviated as Man-**b**-(1 → 6)-Man-**a** (Fig. 1), are presented in Table 1. The ^{1}H NMR assignments of the H-1,2,3,4,5 signals of both residues are in agreement with [21], and the ^{13}C NMR assignments with [22]. Because of severe overlap, the assignment of H-6*pro-R* and H-6*pro-S* for each mannosyl unit was previously not established, but due to the larger chemical shift dispersion in the HMQC spectrum, the H-6 protons could now be identified stereospecifically (Fig. 2). On the Man-**b** C-6 track at δ 61.8 the cross-peaks with Man-**b** H-6*pro-R* and H-6*pro-S* are detected. The observed $J_{5,6}$ values are typical for a *gg*:*gt* equilibrium, whereby the largest coupling constant is expected on H-6*pro-R* [17,23]. Therefore, the resonance at δ 3.74 was assigned to Man-**b** H-6*pro-R* ($J_{5,6pro\text{-}R}$ 6.2 Hz), and that at δ 3.899 to Man-**b** H-6*pro-S* ($J_{5,6pro\text{-}S}$ 2.0 Hz). Because Man-**b** H-6*pro-S* and Man-**b** H-5 resonate outside the bulk signal region, the $J_{5,6pro\text{-}S}$ and $J_{5,6pro\text{-}R}$ values could be obtained very accurately from the 1D spectrum. The HMQC spectrum shows at the Man-**a** C-6 cross-section at δ 66.5, small $J_{5,6}$ coupling constants for both H-6 signals (Fig. 2), which is characteristic for a high *gg* population [24]. Comparison of the chemical shifts of the Man-**a** H-6 atoms with those of the same atoms in α-D-Man*p*-(1 → 6)-β-D-Man*p*1-OMe (**3**), stereospecifically deuterated at C-6 of the 6-linked mannosyl unit [23], afforded the assignment of Man-**a** H-6*pro-R* at 3.977 ppm and Man-**a** H-6*pro-S* at 3.76 ppm. Through simulation of the Man-**a** subspectrum, coupling constants of approximately $J_{5,6pro\text{-}S}$ 1.9 Hz and $J_{5,6pro\text{-}R}$

Table 1
^{1}H and ^{13}C chemical shifts of α-D-Man*p*-(1 → 6)-α-D-Man*p*1-OMe [Man-**b**-(1 → 6)-Man-**a**] at 285 K

Compound	^{1}H Chemical shift (δ)							
	1	2	3	4	5	6*pro-S*	6*pro-R*	OMe
Man-**b**	4.909	3.989	3.850	3.647	3.710	3.899	3.74	
Man-**a**	4.752	3.939	3.75	3.74	3.75	3.76	3.977	3.401
	^{13}C Chemical shift (δ)							
	1	2	3	4	5	6		OMe
Man-**b**	100.3	70.8	71.5	67.7	73.6	61.8		
Man-**a**	101.8	70.8	71.5	67.4	71.6	66.5		55.7

Fig. 2. The HMQC spectrum of α-D-Man*p*-(1 → 6)-α-D-Man*p*1-OMe showing the bulk region. The insets show the cross-sections for Man-**a** C-6 and Man-**b** C-6.

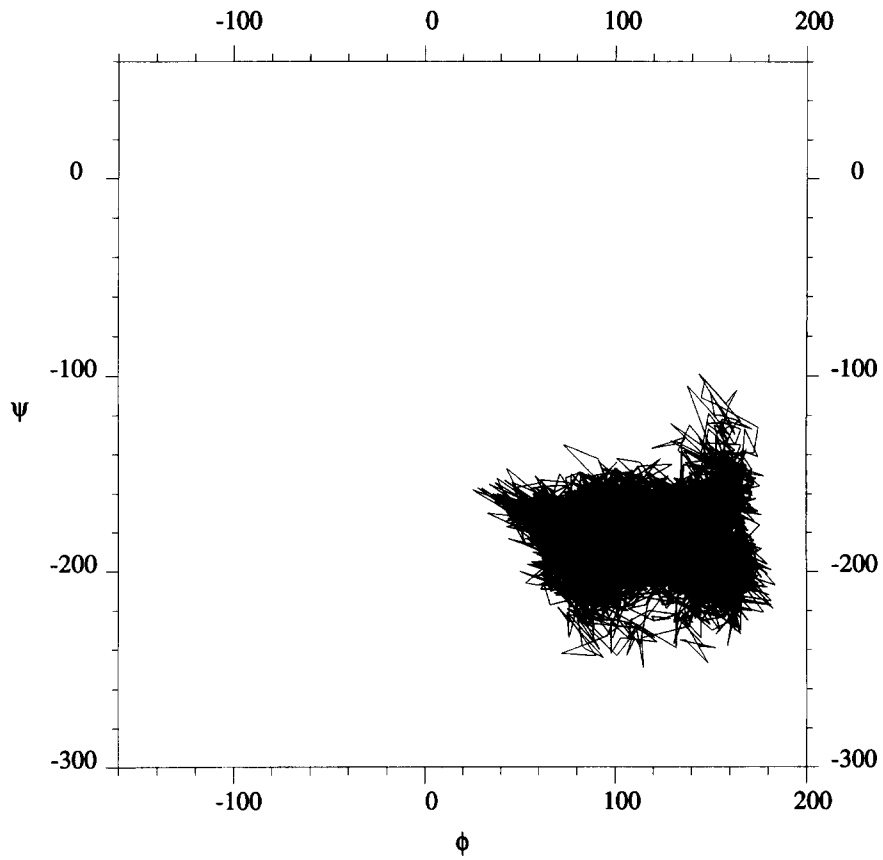

Fig. 3. Molecular dynamics 500-ps trajectory; for Man-**a** the *gg* conformer, for Man-**b** the *gg* conformer.

2.2 Hz were obtained, and only these two small coupling constants can reproduce the pattern found in the HMQC cross-section for Man-**a** C-6.

As discussed above, the HMQC cross-sections of Man-**a** C-6 and Man-**b** C-6 with the

Table 2
Averaged ϕ/ψ minima for different combinations of Man-**a** and Man-**b** rotamer conformations

Compound		Averaged ϕ/ψ minima		
Man-**b**	Man-**a**	Min1	Min2	Min3 (35ps)
gt	*gg*	94/−178		
gg	*gg*	95/−178	140/−185	
gg	*gt*	97/−172	147/−180	90/95

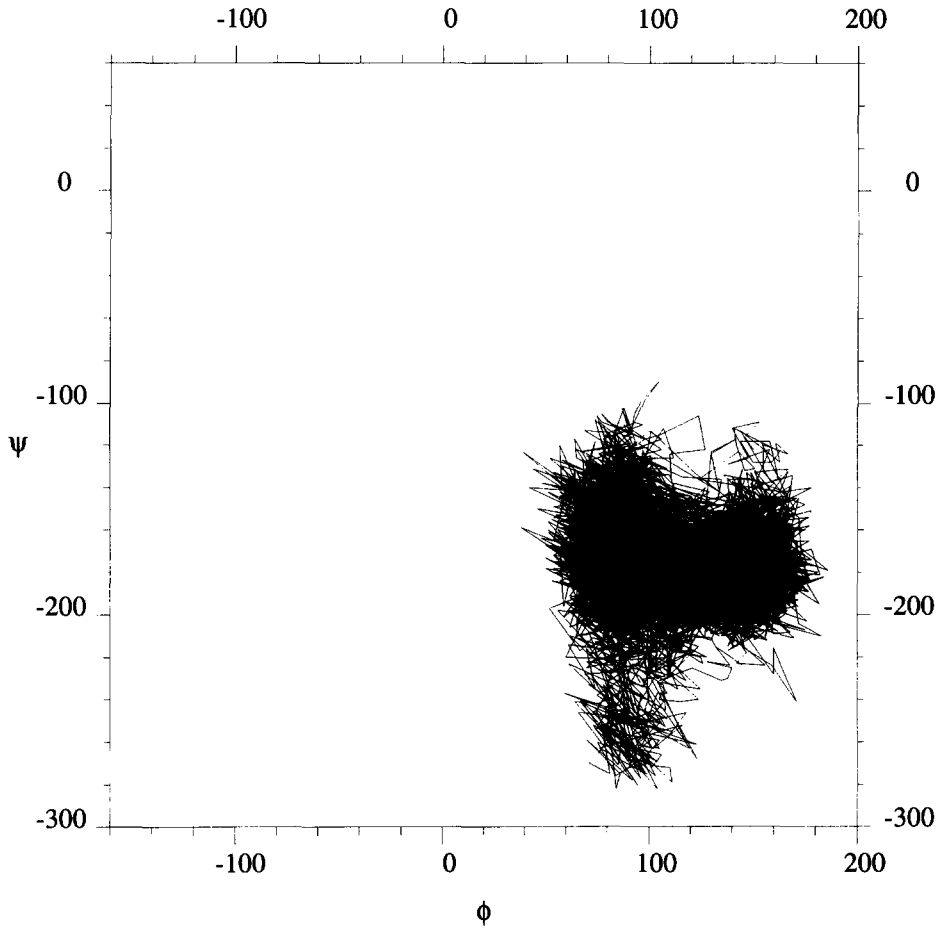

Fig. 4. Molecular dynamics 500-ps trajectory; for Man-**a** the *gt* conformer, for Man-**b** the *gg* conformer.

dissimilar $J_{5,6pro\text{-}S}$ and $J_{5,6pro\text{-}R}$ coupling patterns for H-6*proS* and H-6*proR*, respectively, clearly demonstrate that the rotamer populations for the 6-substituted and the terminal mannosyl residue are different (Fig. 2). In the case of Man-**b** the coupling

Table 3
Selected ϕ/ψ minima of the trajectory were averaged at different rotamer combinations to give different sets of averaged model structures

Compound		Averaged sets of trajectory	
Man-**b**	Man-**a**	Min1	Min2
gt	*gg*	I	
gg	*gg*	II	III
gg	*gt*	IV	V

constants of $J_{5,6pro\text{-}S}$ (2.0 Hz) and $J_{5,6pro\text{-}R}$ (6.2 Hz) correspond to a rotamer ratio of $gg:gt:tg = 0.49:0.55:-0.04$. For Man-**a** the coupling constants $J_{5,6pro\text{-}S}$ (1.9 Hz) and $J_{5,6pro\text{-}R}$ (2.2 Hz) indicate ratios of $gg:gt:tg = 0.97:0.06:-0.03$. The occurrence of virtually one conformation for the Man-**a** residue is in contradiction to published data for this moiety [1].

The MD simulations of **1** showed transitions between $\phi,\psi = 95/-178$ and $\phi,\psi = 140/-185$, whatever minimum from the database [3] with a *gg* conformer for Man-**b** was chosen as starting conformation. As a typical example, in Fig. 3 an MD simulation for **1** with *gg* conformers for both Man-**a** and Man-**b** is depicted. The observed averaged minima were slightly different for the different rotamer population combinations of Man-**a** and Man-**b** as shown in Table 2. In the case where Man-**a** as well as Man-**b** possess the *gg* conformation, transitions between minimum 1 and 2 are observed. In the case of a *gg* conformation for Man-**a** and a *gt* conformation for Man-**b**, minimum 1 is detected exclusively. In only one run, minimum 3 (Egt2) is

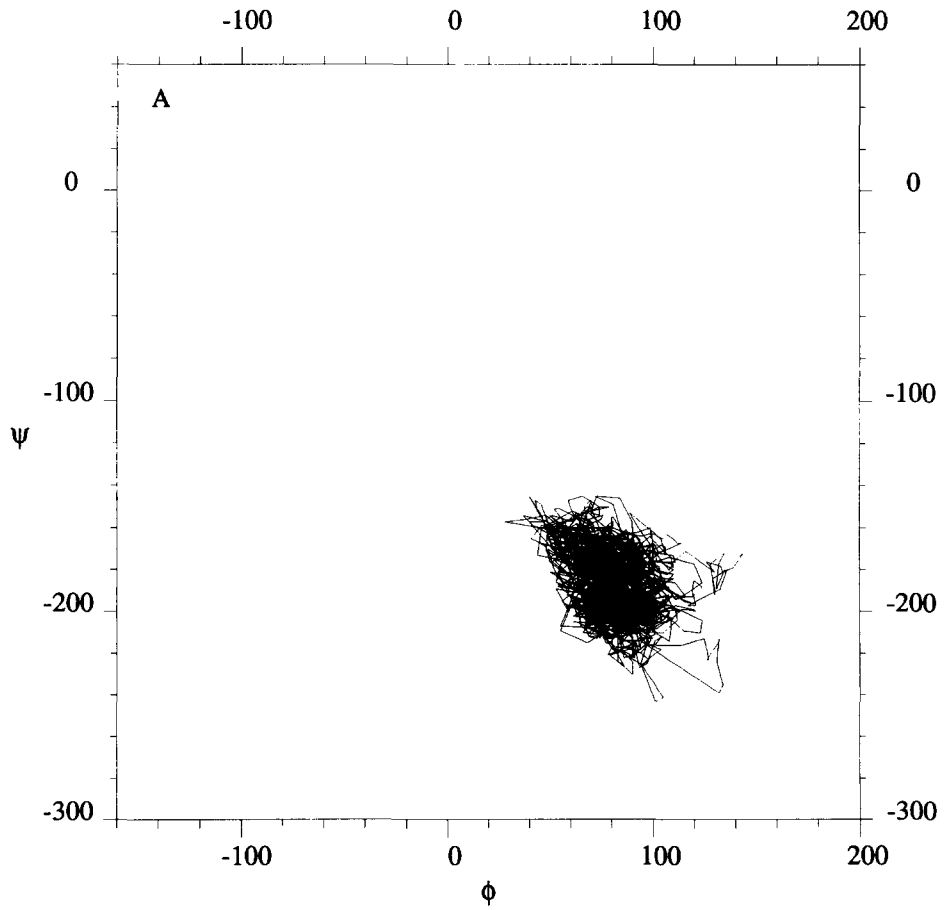

Fig. 5. Same trajectory as in Fig. 3: A, set II at $95/-178$; and B, set III at $140/-185$.

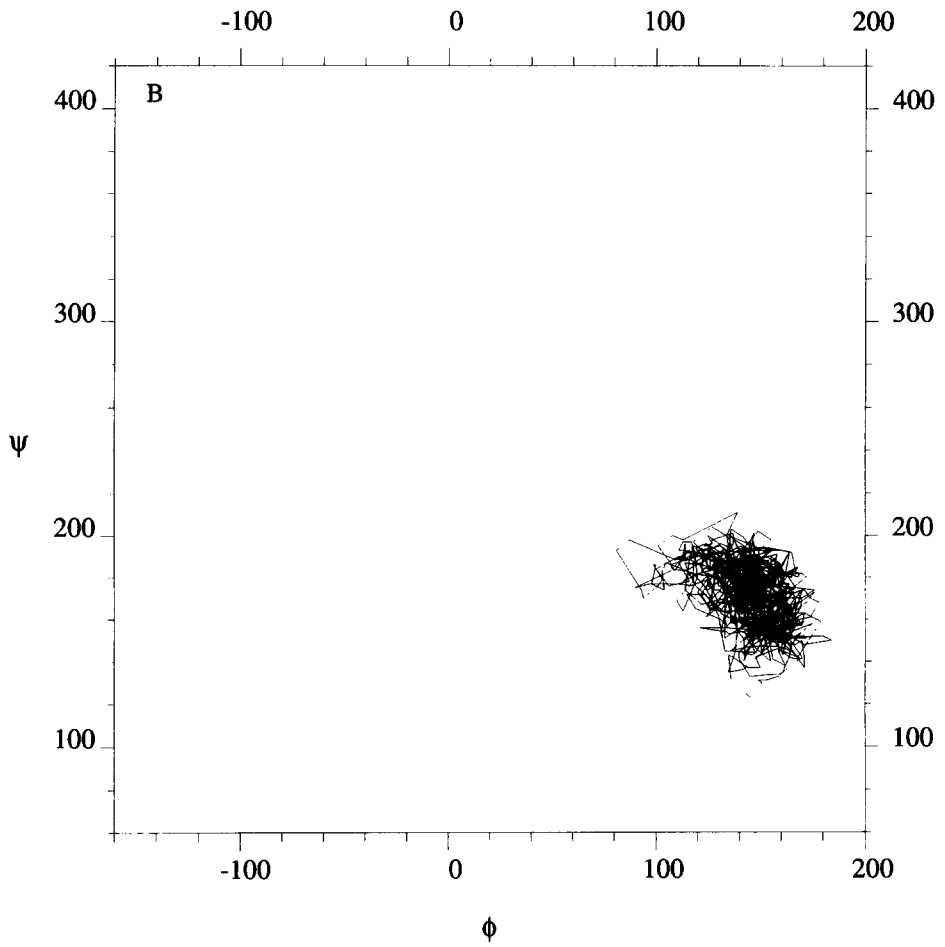

Fig. 5 (continued).

temporarily occupied (Fig. 4; Table 2), but only from 250 to 285 ps. Before and after this interval the trajectory shows only transitions between minima 1 and 2. Minimum 3 has been found to occur in a xylose-type structure for the α-Man-(1 → 6)-β-Man linkage [25]. The minimum at $\phi/\psi = 140/-185$ was not encountered in the MM study, but might be important in removing the discrepancies which were previously found for this linkage between the observed NOEs and the calculated potential energy minima [2,26,27].

Selected parts of the trajectories were averaged to create different sets of model structures, reflecting the different ϕ/ψ minima from Table 2 (see Table 3). In Fig. 5, trajectory II and III are depicted. For CROSREL analysis these models are combined in the calculated rotamer ratios, namely, for Man-**a** $gg:gt = 0.96:0.04$ and for Man-**b** $gg:gt = 0.47:0.53$.

Table 4
Inter- and intra-residue cross-peaks present in the ROE spectra: intra stands for intra-residue cross-peaks which are used for calibration, inter stands for inter-residue cross-peaks which contain conformational information

Protons	Cross-peaks in the ROE spectra	
	intra	inter
a H-1	**a** H-2	
a H-2	**a** H-1	
H_{bulk} [a]		**a** H-6*pro-R* and **b** H-2 [b]
H_{bulk} [a]		**b** H-1
H_{bulk} [a]		**b** H-6*pro-S*
a H-6*pro-R* and **b** H-2 [b]		H_{bulk}
a H-6*pro-R* and **b** H-2 [b]		**b** H-1
a H-6*pro-R* and **b** H-2 [b]		**b** H-3
b H-1	**b** H-3	H_{bulk}
b H-1		**a** H-6*pro-R* and **b** H-2 [b]
b H-3	**b** H-1	**a** H-6*pro-R* and **b** H-2 [b]
b H-6*pro-S*		H_{bulk}

[a] H_{bulk} stands for **a** H-3, **a** H-4, **a** H-5, **a** H-6*pro-S*, **b** H-5, and **b** H-6*pro-R* which could not be separated in the 2D spectra.
[b] **a** H-6*pro-R* and **b** H-2 could not be separated in the 2D spectra.

In Table 4 the intraresidue ROE cross-peaks are summarized which have been used for calibration of τ_c. For the evaluation of the quality of the model the inter- and intra-residue cross-peaks have been used. All ROE intensities were calculated using a τ_c value of 0.106 ns. The distances in the trajectories were averaged to give one model structure as a $< r^{-3} >$ or $< r^{-6} >$ average. The $< r^{-3} >$ average gave slightly better results, which is expected for a fast rotating molecule with fast internal motions [28].

To test if minimum 2 at $\phi/\psi = 140/-185$ could be an artefact, the averaged models for sets I, II, and IV were combined in the calculated rotamer population ratios (Table 3). A better R_w value was obtained when sets III and V were included, therefore it was concluded that minimum 2 provides a real contribution in the structural analysis. The minima 1 and 2 in a 1:1 ratio gave the lowest R_w value and the calculated and observed buildup curves for this ratio are shown in Fig. 6.

Previously, it had been noticed [29] that the $J_{5,6}$ values for αMan-(1 → 6)-αMan and αMan-(1 → 6)-βMan linkages are slightly different, suggesting that differences should exist in the rotamer populations, although the shape of the ϕ/ψ energy contour plot is assumed to be the same [2,3]. Information about the rotamer population of the glycosidic linkage in **3** is available from previous studies [27], showing an equilibrium of $gg:gt:tg = 58.1:40.6:1.3$ (with $J_{5,6pro\text{-}R}$ 6.0 Hz and $J_{5,6pro\text{-}S}$ 2.0 Hz) and a ϕ/ψ minimum around $70/-170$. A NMR study using **3**, stereospecifically deuterated at C-6, showed an equilibrium of $gg:gt:tg = 58:42:0$ with $J_{5,6pro\text{-}R}$ 5.6 Hz and $J_{5,6pro\text{-}S}$ 1.9 Hz [23]. Here, the ϕ/ψ minimum was found to be around $60/-180$. When MD simulations for the α-D-Man*p*-(1 → 6)-β-D-Man*p*1-OMe (**3**) were performed, the same two minima were observed as for **1** (Fig. 7).

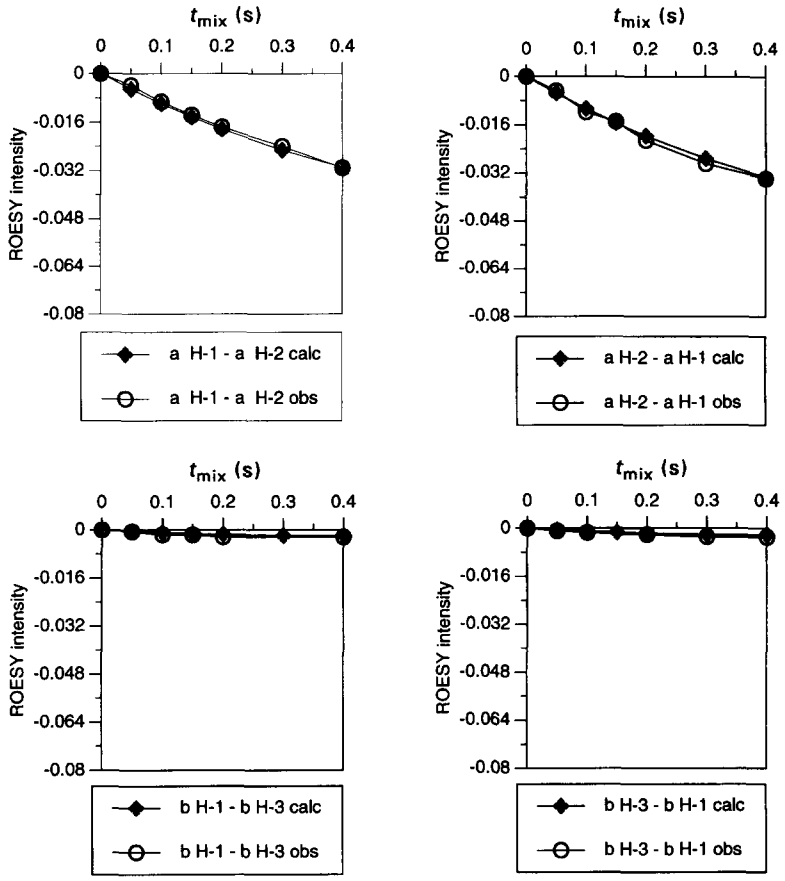

Fig. 6. Calculated and observed buildup curves for the ROE intensities at all mixing times. All buildup curves are plotted on the same scale to facilitate comparison, except for the cross-peak intensity between H_{bulk} and **b** H6*pro-S* which is plotted on a larger scale.

4. Discussion

A generally applied approach to the conformational analysis of larger glycans is to study separately small oligosaccharide fragments. The results are then used to construct, from these building blocks, the overall structure of a larger glycan. From this point of view α-D-Man*p*-(1 → 6)-α-D-Man*p*1-OMe was studied here, since this fragment is crucial for the overall conformation of larger oligomannose and hybrid type N-linked glycans. A detailed description of the conformational behaviour of this disaccharide in solution is a prerequisite to using it as a building block. By a combination of HMQC spectroscopy, ROE buildup curves, molecular dynamics simulations, and the CROSREL program, this conformation, previously difficult to define, could be elucidated. The flexibility of the (1 → 6) linkage is assessed in detail by MD, and the HMQC

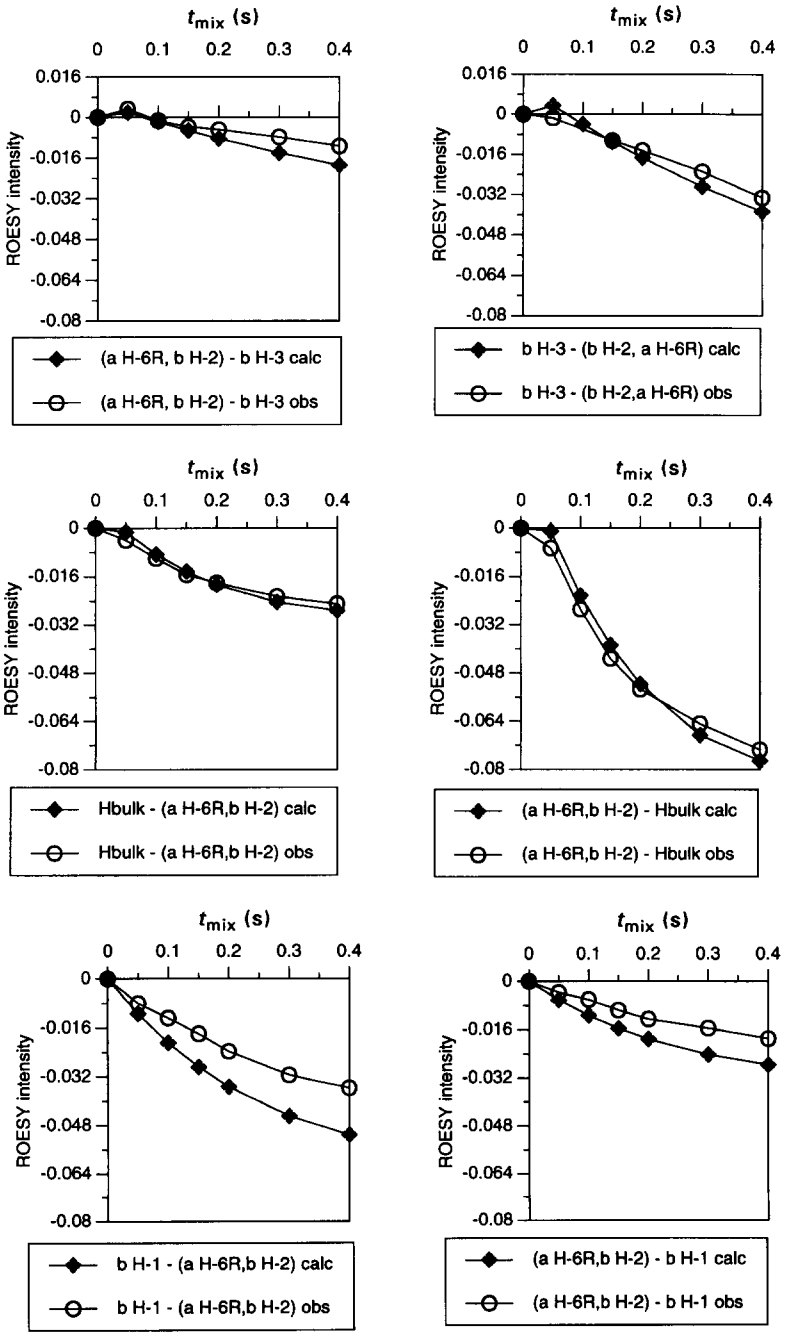

Fig. 6 (continued).

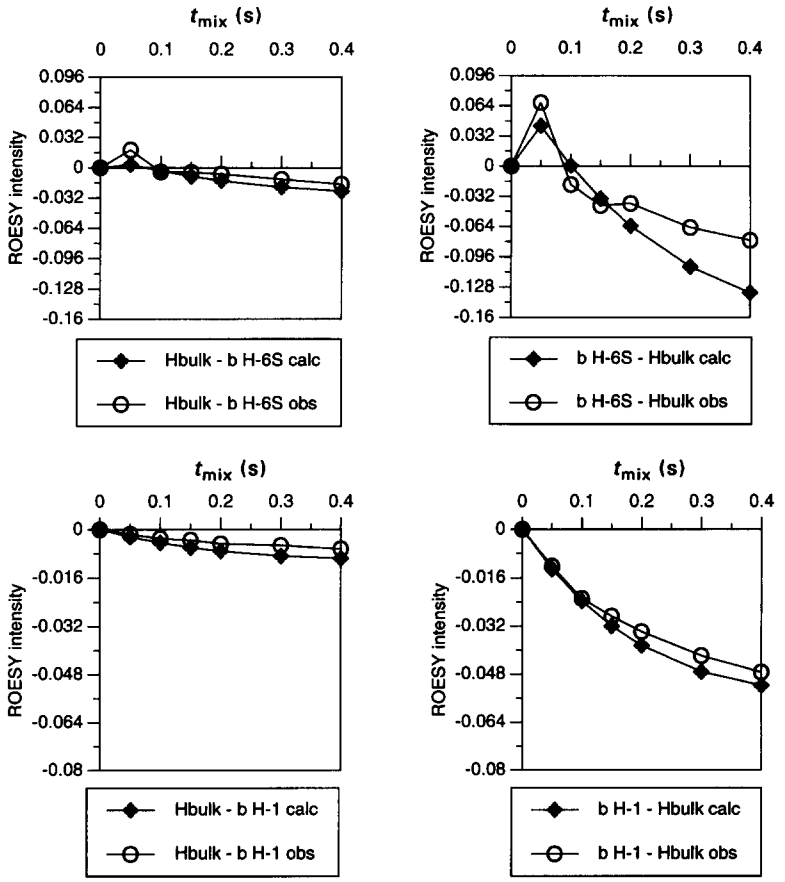

Fig. 6 (continued).

experiment proved to be instrumental in determining the coupling constants $J_{5,6pro\text{-}R}$ and $J_{5,6pro\text{-}S}$.

In the present study it is demonstrated that MM calculations, in vacuum, yield several redundant minima for this disaccharide. However, MD simulations gave rise to an additional minimum, not present in the MM studies. This minimum at ϕ/ψ 140/−185 has to be included in the conformational analysis. More flexibility is observed for ϕ than for ψ, in contrast to a previous proposal [1,2,4,6]. The accessible ψ region in the database published by Imberty et al. [3] is very broad. However, these conformations (Egg2–Egg4) are not stable under the conditions described here. It is very likely that the second minimum is stabilized by the solvent. Analysis of intramolecular hydrogen bonds, and of those bridged by one water molecule, provided no proof of the existence of these kinds of bonds. Therefore, we hypothesize a network of water molecules to stabilize the second minimum, and to explain the preference for the *gg* rotamer over the *gt* rotamer.

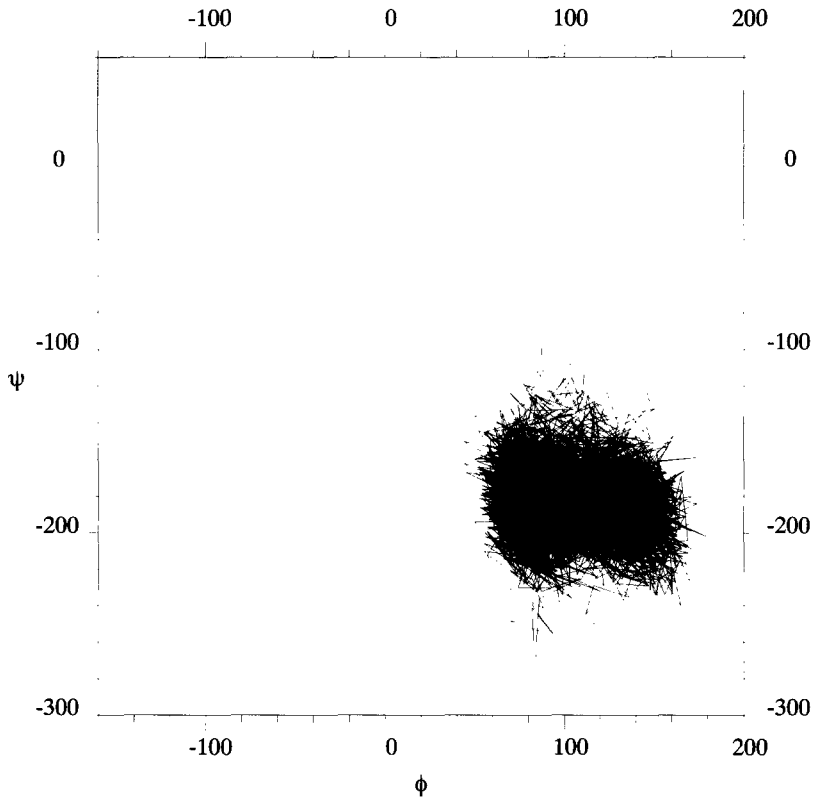

Fig. 7. Molecular dynamics 500-ps trajectory for α-D-Man*p*-(1 → 6)-β-D-Man*p*1-OMe (**3**).

The program CROSREL [18,19] proved to be very useful to estimate τ_c and to compare experimental ROESY buildup curves with those from a model structure. The presence of almost exclusively the *gg* conformer for the (1 → 6) linkage was an unexpected result, because previous data suggested a 1:1 ratio for *gg* and *gt*. As a consequence the rotamer population of the (1 → 6) linkage has to be evaluated separately in each glycan, and it does not seem possible to predict rotamer populations for larger glycans on the basis of data from smaller oligosaccharides as building blocks. Even for smaller oligosaccharides large differences can exist. For example in α-D-Man*p*-(1 → 6)[α-D-Man*p*-(1 → 3)]-α-D-Man*p*1-OMe, a *gg*:*gt* ratio of 1:1 for the αMan-(1 → 6)-αMan linkage has been demonstrated [1], so a relatively small change in the overall structure can induce a large change in rotamer population. It has been proposed that rotamer populations are affected by steric restrictions due to side chains present in the oligosaccharide [5]. This proposal has no general validity because such side chains are not present in **1** investigated in the current study.

Acknowledgements

This work has been supported by the Netherlands Foundation for Chemical Research (SON/NWO). A. Rivera-Sagredo was supported by the Spanish Consejo Superior de Investigaciones Científicas with a post-doctoral fellowship. We thank Drs B.R. Leeflang and L.M.J. Kroon-Batenburg for many stimulating discussions and assistance with the CROSREL program, and Dr J.G.M. van der Ven for the generous gift of the methyl glycoside.

References

[1] J.R. Brisson and J.P. Carver, *Biochemistry*, 22 (1983) 1362–1368.
[2] S.W. Homans, A. Pastore, R.A. Dwek, and T.W. Rademacher, *Biochemistry*, 26 (1987) 6649–6655.
[3] A. Imberty, S. Gerber, V. Tran, and S. Pérez, *Glycoconjugate J.*, 7 (1990) 27–54.
[4] J.R. Brisson and J.P. Carver, *Biochemistry*, 22 (1983) 3680–3686.
[5] S.W. Homans, R.A. Dwek, J. Boyd, M. Mahmoudian, W.G. Richards, and T.W. Rademacher, *Biochemistry*, 25 (1986) 6342–6350.
[6] T. Peters and T. Weimar, *J. Biomol. NMR*, 4 (1994) 97–116.
[7] D. Marion and K. Wüthrich, *Biochem. Biophys. Res. Commun.*, 113 (1983) 967–974.
[8] A.A. Bothner-By, R.L. Stephens, J-M. Lee, C.D. Warren, and R.W. Jeanloz, *J. Am. Chem. Soc.*, 106 (1984) 811–813.
[9] A. Bax and D.G. Davis, *J. Magn. Reson.*, 63 (1985) 207–213.
[10] A. Bax, R.H. Griffey, and B.L. Hawkins, *J. Magn. Reson.*, 55 (1983) 301–315.
[11] R.A. Hoffmann, J.P. Kamerling, and J.F.G. Vliegenthart, *Carbohydr. Res.*, 226 (1992) 303–311.
[12] IUPAC-IUB JCBN, Symbols for specifying the conformation of polysaccharide chains (Recommendations 1981), *Eur. J. Biochem.*, 131 (1983) 5–7.
[13] W.F. van Gunsteren and H.J.C. Berendsen, Groningen Molecular Simulation (GROMOS) Library Manual, University of Groningen, The Netherlands, 1987.
[14] J. Koehler, W. Saenger, and W.F. van Gunsteren, *Eur. Biophys. J.*, 15 (1987) 197–210.
[15] W.F. van Gunsteren and H.J.C. Berendsen, *Mol. Phys.*, 34 (1977) 1311–1327.
[16] C.A.G. Haasnoot, F.A.A.M de Leeuw, and C. Altona, *Tetrahedron*, 36 (1980) 2783–2792.
[17] Y. Nishida, H. Hori, H. Ohrui, and H. Meguro, *J. Carbohydr. Chem.*, 7 (1988) 239–250.
[18] L.M.J. Kroon-Batenburg, J. Kroon, B.R. Leeflang, and J.F.G Vliegenthart, *Carbohydr. Res.*, 245 (1993) 21–42.
[19] B.R. Leeflang and L.M.J. Kroon-Batenburg, *J. Biomol. NMR*, 2 (1992) 495–518.
[20] C. Gonzalez, J.A.C. Rullmann, A.M.J.J. Bonvin, R. Boelens, and R. Kaptein, *J. Magn. Reson.*, 91 (1991) 659–664.
[21] J.R. Brisson, F.M. Winnik, J.J. Krepinsky, and J.P. Carver, *J. Carbohydr. Chem.*, 2 (1983) 41–55.
[22] T. Ogawa and K. Sasajima, *Carbohydr. Res.*, 97 (1981) 205–227.
[23] H. Hori, Y. Nishida, H. Ohrui, H. Meguro, and J. Uzawa, *Tetrahedron Lett.*, 29 (1988) 4457–4460.
[24] J.P. Carver, in V. Ginsburg and P.W. Robbins (Eds.), *Biology of Carbohydrates*, Wiley, New York, 1984, pp 289–331.
[25] J.P.M. Lommerse, Thesis, Utrecht University, 1994.
[26] D.A. Cumming and J.P. Carver, *Biochemistry*, 26 (1987) 6664–6676.
[27] D.A. Cumming and J.P. Carver, *Biochemistry*, 26 (1987) 6676–6683.
[28] J. Tropp, *J. Chem. Phys.*, 72 (1980) 6035–6043.
[29] E. Berman, *Eur. J. Biochem.*, 165 (1987) 385–391.